Acta Crystallographica Section B
Structural Science
ISSN 0108-7681

X-ray diffraction study of the phase transitions of $(CH_3)_4NCdCl_3$ between 293 and 80 K: a quantitative analysis of the ferroelastic domains distribution below 118 K

I. Peral,[a]* G. Madariaga,[a] A. Pérez-Etxebarria[a] and T. Breczewski[b]

[a]Departamento de Física de la Materia Condensada, Facultad de Ciencias, Universidad del País Vasco, Apdo 644, 48080 Bilbao, Spain, and [b]Departamento de Física Aplicada II, Facultad de Ciencias, Universidad del País Vasco, Apdo 644, 48080 Bilbao, Spain

Correspondence e-mail: wmbpeali@lg.ehu.es

Received 28 July 1999
Accepted 22 October 1999

X-ray diffraction patterns of $[N(CH_3)_4][CdCl_3]$, tetramethylammonium trichlorocadmate(II), have been investigated in the temperature range 80–293 K, which includes two phase transitions at 118 and 104 K, respectively. The main interest in this compound is to establish the mechanism of the structural phase transitions common to other members of the isostructural family $[(CH_3)_4N][MX_3]$. It is supposed to be related to the ordering of the organic part together with some small distortion of the inorganic chains. The origin of the order–disorder mechanism would be the orientationally disordered distribution of the tetramethylammonium tetrahedra at room temperature. Maximum Entropy Methods suggest that the most probable distribution of the organic groups can be described through the so-called two-well model, in which one threefold axis of the tetramethylammonium tetrahedron coincides with the crystallographic threefold axis of the structure. Below 118 K the reflections are split. However, the splitting cannot be fully explained by the ferroelastic domains expected to appear after the phase transitions. Recent NMR results [Mulla-Osman *et al.* (1998). *J. Phys. Condensed Matter*, **10**, 2465–2476] corroborate the existence of more domains than expected from symmetry considerations. A model of ferroelastic domains which is in agreement with both X-ray diffraction diagram and NMR measurements is proposed.

1. Introduction

The compound $[(CH_3)_4N][CdCl_3]$ [TMCC, tetramethylammonium trichlorocadmate(II)] belongs to the isostructural family $[(CH_3)_4N][MX_3]$ (M: divalent metal = Cd, Mn, Ni, Cu, V, Pb; X: halogen = Cl, Br, I). The structure of most of these compounds at room temperature (phase I) is assumed to be due to the superposition of two lattices with the same periodicity and space group $P6_3/m$ ($Z = 2$). One of these lattices is built from linear chains (along **c**) of stacked $CdCl_6$ octahedra sharing faces, whereas the other lattice is formed by tetrahedral tetramethylammonium (TMA) ions located between the chains. All these compounds undergo several structural phase transitions as the temperature decreases. In the case of TMCC, two successive structural first-order phase transitions have been observed at 118 and 104 K, respectively. The former connects phase I with a monoclinic structure with space group $P2_1/m$ and $Z = 2$ (phase II). The latter leads to another monoclinic phase (phase III) with space group $P2_1/b$ with $Z = 12$. Considerable effort has been made to explain the

transition mechanism which is commonly associated with ordering processes involving TMA groups, without important modifications in the inorganic chains. The structural reason lies within the incompatibility between the ideal molecular symmetry ($\bar{4}3m$) and the site symmetry ($3/m$) corresponding to the special positions occupied by the centres (N atoms) of the

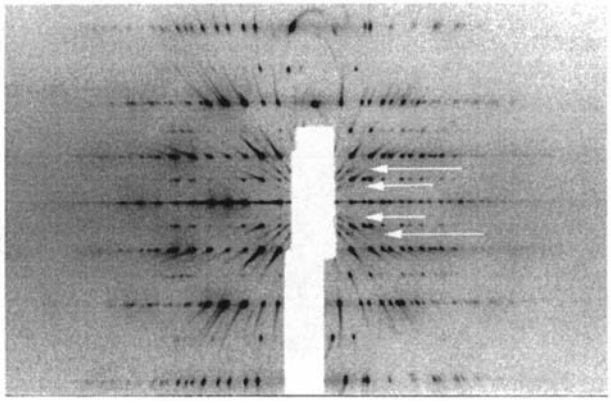

Figure 1
Oscillation photograph at room temperature around the **c** axis showing both the $\{a_1^*, b_1^*, c_1^*\}$ and $\{a_2^*, b_2^*, c_2^*\}$ reciprocal lattices. Layers belonging to the second lattice (marked with arrows) are rather diffuse and only appear in a small range of θ.

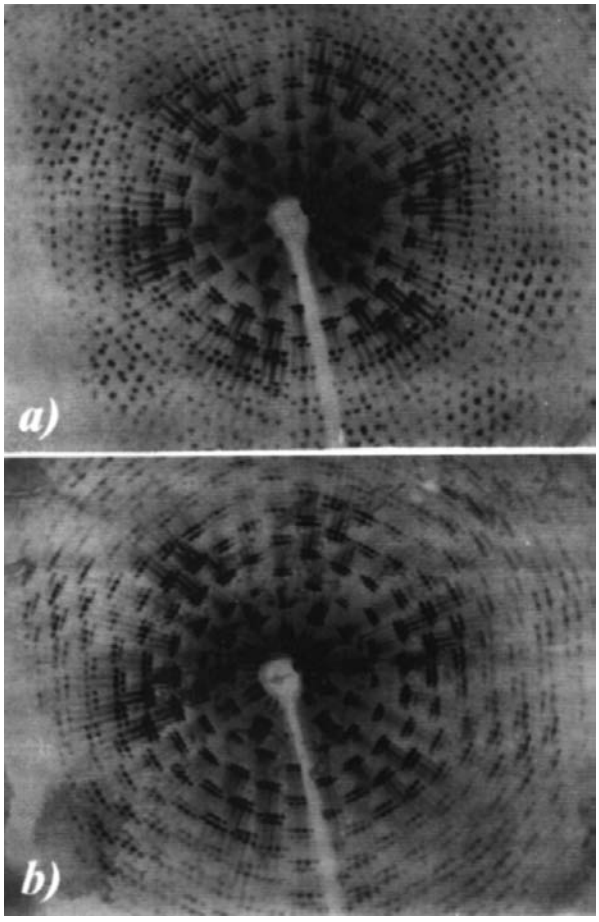

Figure 2
(*a*) Mo $K\alpha$ precession photograph of the ($hk0$) plane at 103 K. (*b*) Same photograph at 80 K.

Table 1
Experimental details.

Crystal data	
Chemical formula	$C_4H_{12}N{\cdot}CdCl_3$
Chemical formula weight	292.62
Cell setting	Hexagonal
Space group	$P6_3/m$
a (Å)	9.126 (5)
b (Å)	9.126 (5)
c (Å)	6.718 (2)
α (°)	90.000 (9)
β (°)	90.000 (9)
γ (°)	120.00 (1)
V (Å^3)	484.5 (6)
Z	2
D_x (Mg m^{-3})	2.008
Radiation type	Mo $K\alpha$
Wavelength (Å)	0.71073
No. of reflections for cell parameters	25
θ range (°)	4–25
μ (mm^{-1})	2.99
$\sin\theta/\lambda_{max}$ (Å^{-1})	0.993
Temperature (K)	293
Crystal form	Hexagonal prism
Crystal size (mm)	0.285 × 0.12 × 0.09
Crystal colour	Colourless
Data collection	
Diffractometer	CAD-4
Data collection method	$\theta/2\theta$ scans
Scan width (°)	0.8 + 0.35tan θ
Scan speed (° min^{-1}): min/max	0.686/4.12
Absorption correction	Analytical
T_{min}	0.7089
T_{max}	0.7880
No. of measured reflections	2979
No. of independent reflections	1406
No. of observed reflections	791
Criterion for observed reflections	$I > 3\sigma(I)$
R_{int}	0.021
θ_{max} (°)	44.91
Range of h, k, l	$0 \rightarrow h \rightarrow 15$ $0 \rightarrow k \rightarrow 15$ $-13 \rightarrow l \rightarrow 13$
No. of standard reflections	3
Frequency of standard reflections	Every 60 min
Intensity decay (%)	3
Refinement	
Refinement on	F
R	0.045
wR	0.031
S	0.87
No. of reflections used in refinement	791
No. of parameters used	29
H-atom treatment	undef
Weighting scheme	$1/\sigma^2(F)$
$(\Delta/\sigma)_{max}$	0.363
$\Delta\rho_{max}$ (e Å^{-3})	1.511
$\Delta\rho_{min}$ (e Å^{-3})	−4.813
Extinction method	None
Source of atomic scattering factors	*International Tables for X-ray Crystallography* (1974, Vol. IV, Tables 2.2B and 2.3.1)
Computer programs	
Data collection	*CAD*-4*VPC* (Enraf–Nonius, 1996)
Cell refinement	*CAD*-4*VPC* (Enraf–Nonius, 1996)
Data reduction	*Xtal*3.2 (Hall *et al.*, 1992)
Structure solution	*Xtal*3.2 (Hall *et al.*, 1992)
Structure refinement	*XtalCRYLSQ* (Olthof-Hazekamp, 1992)
Preparation of material for publication	*XtalBONDLACIFIO* (Dreissing *et al.*, 1992; Hall, 1992)

TMA ions. They are forced to be statistically disordered among the several orientations related by those crystallographic elements not belonging to the intersection of both point groups. This picture of the orientational disorder of TMA groups is basically supported by the refined structures of some compounds of the family in which the C atoms positions are usually split in 2, 3 or 6 symmetry-related positions. Nevertheless, X-ray or neutron elastic scattering cannot distinguish whether the refined positions come from disorder of dynamical character or from a space averaging. A common way of describing the orientational disorder in TMA groups has been the Frenkel model, in which the molecules jump among a finite number of equally probable orientations. In the case of TMCC and related compounds, different Frenkel models have been considered.

(i) A two-well model (2W) in which one threefold axis of the TMA tetrahedron coincides with the crystallographic threefold axis, so that the full symmetry of the site is reached by superimposition of two equiprobable orientations related to each other by the m_z symmetry operation (Morosin & Graeber, 1967; Morosin, 1972; Peercy *et al.*, 1973).

(ii) A three-well model (3W) in which one mirror plane of the TMA tetrahedron coincides with the crystallographic mirror plane, so that the threefold axis of the site relates three equiprobable orientations (Jewess, 1982).

(iii) A six-well model (6W) in which the C atoms of TMA groups are in general positions, so that both the crystallographic threefold axis and the mirror plane of the site are statistical symmetry elements that generate six possible orientations (Couzi & Mlik, 1986).

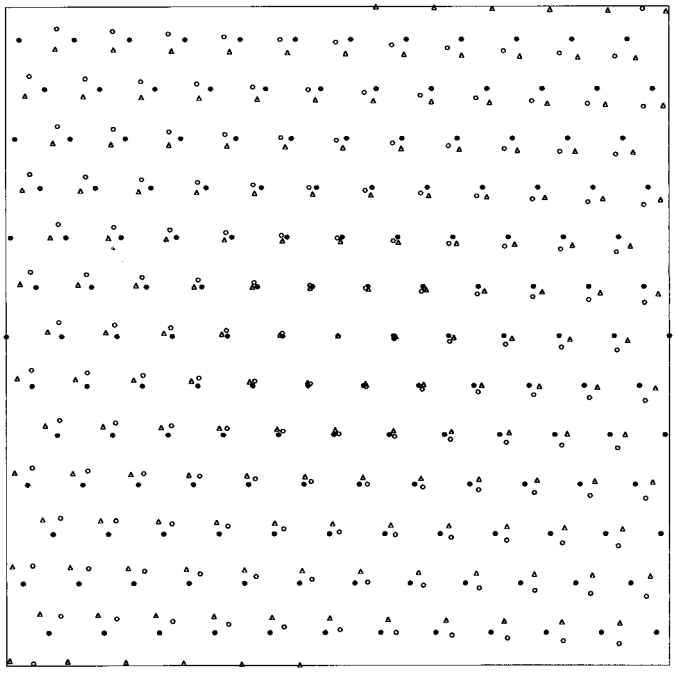

Figure 3
Expected appearance of any reciprocal plane perpendicular to $\mathbf{c}^*$ of phase II, assuming the loss of the threefold axis in the phase transition that relates phases I and II. (●) Reciprocal lattice points of the first ferroelastic domain. (△) Reciprocal lattice points of the second ferroelastic domain, related to the first one by a rotation of 120°. (○) Reciprocal lattice points of the third ferroelastic domain, related to the first one by a rotation of 240°.

Table 2
Measured angles (°) between the c^* axis of the strongest twin and the weaker ones detected at room temperature in several samples (see text).

S_i (i = 1, 2, 3, 4) are arbitrary labels for the different samples. The subscripts given for each angle [α_i (i = 1, 2, 3)] are arbitrary labels for the weak twins.

Sample	α_1	α_2	α_3
S_1	76		
S_2	55	85	
S_3	63	18	63
S_4	67	10	

Other microscopic techniques, such as incoherent quasi-elastic neutron scattering, require 24 sites to explain the ordering of the organic tetrahedra, which is modelled by the freezing of a flip motion between two positions related by the mirror plane m_z (Rodriguez, Guillaume & Couzi, 1996). This soft-mode behaviour has not been confirmed by other techniques such as Raman scattering (Mlik & Couzi, 1982). Moreover, Raman measurements also suggest that the ordering of TMA cannot be the only mechanism for the phase transitions of TMCC.

A structural solution of the low-temperature phases could confirm the proposed phase transition schemes. However, this is not a trivial task since the appearance of ferroelastic domains prevents even a precise determination of the low-temperature space groups and only the low-temperature structures of $[(CH_3)_4N][MnCl_3]$ (Braud *et al.*, 1990; Rodriguez, Aguirre-Zamalloa, 1996) and $[(CH_3)_4N][CdBr_3]$ (Aguirre-Zamalloa *et al.*, 1993) are known. For this latter (particularly favourable) compound the order–disorder character of the phase transition has been established.

The aim of this work is to present and interpret the diffraction patterns of TMCC in phases I, II and III. At room temperature (phase I) the measured samples are composed of several not superimposed isostructural domains with no symmetry relation among them. Although there are no differences among the different refined models (2W, 3W and 6W) for the orientational disorder of the organic tetrahedra, the maximum entropy criteria favours the 2W model. The domain structures of phases II and III cannot be fully explained using the 'classical' group-theoretical rule (see, for example, Salje, 1990) for calculating the number of ferroelastic domains, even if the space groups of all phases are reconsidered. Nevertheless, the correct number and orientation of ferroelastic domains can be easily calculated (Shuvalov *et al.*, 1985). This general domain distribution is not a specific feature of TMMC, but it is also present in many different compounds.

2. Experimental

Colourless, hexagonal prismatic crystals of TMCC were grown by slow evaporation at 315 K of a saturated aqueous solution, prepared with stoichiometric amounts of $N(CH_3)_4Cl$ and

$CdCl_2$. In addition, several samples used for NMR measurements (Mulla-Osman *et al.*, 1998) were kindly supplied by D. Michel at the University of Leipzig. Single crystals of TMCC have been studied with Weissenberg and precession techniques (using filtered Mo $K\alpha$ and Cu $K\alpha$ radiation), as well as with a four-circle Enraf–Nonius CAD-4 diffractometer and a Stoe IPDS using monochromated Mo $K\alpha$ radiation.

Monochromatic Cu $K\alpha_1$ X-ray powder measurements were carried out on a Stoe focusing beam transmission diffractometer equipped with a linear position sensitive detector. Samples were prepared by pulverization of the synthesized single crystals. Powder diffraction patterns were collected using the Debye–Scherrer geometry. The scanned region of reciprocal space was (5–110°) in 2θ.

Low-temperature measurements were realised with a nitrogen-gas-flow cooling system (Cosier & Glazer, 1986). The temperature stability was $\pm$ 0.2 K.

3. Description of the single-crystal diffraction data

3.1. Phase I

At room temperature, precession photographs of the reciprocal planes ($hk0$) and ($hk1$) show diffraction diagrams with an intensity distribution nearly hexagonal. A conventional hexagonal metric ($a_1 = b_1$ = 9.2, c_1 = 6.6 Å, γ = 120°) was chosen to index the whole diagram. Only the systematic absences (00ℓ), $\ell = 2n + 1$, were observed in the reciprocal planes ($h0\ell$) and ($h1\ell$). Two space groups are compatible with the diffraction diagrams, $P6_3/m$ and $P6_3$. Pyroelectric measurements (Gesi, 1992) seem to confirm $P6_3/m$ as the space group for phase I, the same reported previously by Morosin (1972). However, a closer inspection of the photographs also shows the presence of very weak reflections located at rather low angles ($\theta < 20°$) and disposed on a new reciprocal lattice incommensurate with that of the strong reflections. The rotational symmetry of these reflections is also closely hexagonal and their reciprocal basic vectors are approximately given by $a_2^* \simeq 0.3a_1^*$, $b_2^* \simeq 0.3b_1^*$, $c_2^* \simeq 0.3c_1^*$, γ = 120°.[1] No systematic absences were detected for the sublattice of weak reflections. A new set of precession photographs using Cu $K\alpha$ radiation and long-exposure Weissenberg photographs confirmed the existence of two mutually incommensurate lattices. An oscillation photograph around the **c** axis is shown in Fig. 1.

Figure 4
(*a*) ($hk0$) plane of one of the weak twins detected at room temperature. Only the reflections appearing at low Bragg angles and showing hexagonal symmetry belong to the selected twin. The strong reflections (marked with a S) belong to the dominant twin (see text).

3.2. Phase II

Phase II was subsequently investigated using several crystals by precession photographs of the reciprocal planes ($hk0$), ($hk1$) and ($h0\ell$) at 103 K. The reciprocal planes perpendicular to **c** show bunches of reflections (see Fig. 2) surrounding the reciprocal points spanned by the basis $\mathbf{a}_1^*$, $\mathbf{b}_1^*$ and $\mathbf{c}_1^*$, indicating the presence of several (expected) domains. The symmetry of this plane is still hexagonal or pseudo-hexagonal with almost no metrical variation. Since the spread of reflections cannot be observed in the ($h0\ell$) plane, the domains must share $\mathbf{c}_1^*$ as the common basic vector. Given the complex spot distribution, only very approximate lattice parameters can be derived from the photographs. More accurate values [a_1 = 9.3340 (17), b_1 = 8.7963 (15), c_1 = 6.6880 (17) Å and γ = 120.958 (13)°] were obtained from the indexation of powder diagrams collected at 103 K. Again the only observed systematic extinction is $(00\ell)_1$, $\ell = 2n + 1$. These results would be in agreement with the space group usually assumed for phase II ($P2_1/m$, Z = 2; Braud *et al.*, 1990), except for an unexpected anomaly: the observed number of points corresponding to each split bunch is as high as 12. Given this result, the temperature was further lowered towards phase III.

3.3. Phase III

At 80 K the aspect of the reciprocal plane ($hk0$) is very similar to that of phase II, see Fig. 2. Again there are groups of 12 reflections now more clearly observed by the effect of temperature decrease, although without any apparent change in their relative intensities. The difference between the diffraction diagrams of phases II and III is a small variation in lattice parameters that makes the distribution of each packet of reflections more compact. The rough reciprocal lattice used for an approximate indexing of the photographs is consistent with the values [a_1 = 8.8 (1), b_1 = 18.4 (1), c_1 = 20.0 (1) Å and γ = 121.0 (5)°] previously published (Braud *et al.*, 1990). Powder patterns collected at 90 K could not be used for the

[1] Hereafter the numbers '1' and '2' will refer to Miller indices and lattice parameters corresponding to the reciprocal sublattices of strong and weak reflections, respectively.

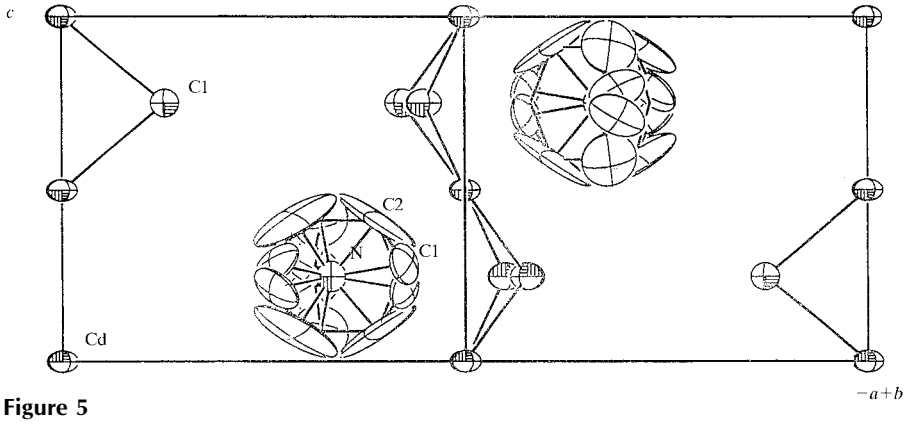

Figure 5
ORTEP (Davenport *et al.*, 1992) projection along [110] of the refined structure (6W) of phase I. The large thermal ellipsoids of C atoms describe three (symmetry-related) arcs, along which the electronic density is distributed. Zigzag lines represent part of the inorganic chains.

refinement of the lattice parameters owing to the great overlapping of the X-ray diffraction peaks. However, the phase transition can be confirmed by the doubling of $\mathbf{b}_1$, the tripling of $\mathbf{c}_1$ (detected by cone-axis photographs along the pseudo-hexagonal direction) and the existence of new extinction rules: $(00\ell)_1$, $\ell = 2n + 1$, and $(hk0)_1$, $k = 2n + 1$. Again the reported space group (Braud *et al.*, 1990) for phase III of TMCC $P2_1/b$ ($Z = 12$) is consistent with these systematic absences. The incommensurate sublattice is still present at 103 and 80 K. However, the number of split spots is again incompatible with the expected number of ferroelastic twin domains (inherited from phase II).

This abnormal result would invalidate the space groups assigned to the three phases, since the anticipated decrease of crystal symmetry should only give rise to three ferroelastic twin domains and therefore to triplets of reflections related by the symmetry elements lost at the transition point (see Fig. 3). Another possible explanation would be the presence in the sample of several misaligned crystals. This point was checked by testing on several samples the relative intensity among the reflections belonging to a certain bunch and the reversibility of the phase transition through several heating/cooling cycles. The same was found with a different wavelength. The surprising number of domains present in the low-temperature phases points (as simpler possibilities) either to a wrong assignation of space groups or to sample-dependent effects owing to bad crystal quality. Since the results were identical for the samples used in NMR experiments (Mulla-Osman *et al.*, 1998), the second possibility can be practically ruled out. The first one will be subsequently commented.

4. Data collection at room temperature

4.1. Analysis of the reciprocal space

The intensities indexed with the reciprocal lattice $\{\mathbf{a}_1^*, \mathbf{b}_1^*, \mathbf{c}_1^*\}$ were collected in the experimental conditions given in Table 1.[2] Using a different (larger) sample, some reflections indexed with the reciprocal lattice $\{\mathbf{a}_2^*, \mathbf{b}_2^*, \mathbf{c}_2^*\}$: [$(\bar{2}00)$, (200), $(0\bar{2}0)$, (020) and $(\bar{2}20)$] were located manually and scanned along $\mathbf{a}_2^*$ and $\mathbf{b}_2^*$. These reflections are rather broad and they could not be automatically centred and used for the refinement of $\mathbf{a}_2^*$, $\mathbf{b}_2^*$ and $\mathbf{c}_2^*$. Only the reflections lying on the $hk0$ plane were collected with an approximate orientation matrix based on the transformation $\mathbf{a}_2^* \simeq 0.3\mathbf{a}_1^*$, $\mathbf{b}_2^* \simeq 0.3\mathbf{b}_1^*$ and $\mathbf{c}_2^* \simeq 0.3\mathbf{c}_1^*$.[3] A careful study of the data shows also that the profiles of the diffracted intensities $(hk\ell)_1$ are slightly split. They seem to be the superposition of at least two reflections that belong to identical reciprocal lattices, but with a different, but very close, orientation. For a better estimation of the splitting, some of the profiles were deconvoluted, fitting them to a maximum of three Gaussians. The calculated shift among the overlapped peaks is very small (0.01° in θ) and remains constant when temperature is decreased. If this small splitting is the origin of the domain structure of phase II, the phase transition should be markedly of first order. Irrespective of the measured sample, data collected using a Stoe IPDS showed the existence of several domains. The twin structure varies from sample to sample, although there is always a strongly dominant domain. On the other hand, the domains do not share any crystallographic direction and there is not a symmetry element that relates them one to each other (Fig. 4). Such distribution precludes the overlap among reflections belonging to different domains, which means that the intensities of each twin have the same information about the structure of the compound. Their orientation relative to the strongest one, given in terms of the angles between the corresponding **c** axes, are in Table 2. As a consequence, they are practically invisible for conventional detectors and therefore it is impossible to relate the observed reciprocal space with the slight splitting of the reflections measured with the CAD4. In this series of measurements the sublattice of weak reflections could not be detected. Several data collections with different samples (for which precession photographs exhibited clearly both reciprocal lattices) and exposure times showed the same results. Given the sensitiveness of the image plate, the absence of the weak reflections should be attributed to some difference in the experimental conditions. It could be finally confirmed that the intensities indexed with the sublattice $\{\mathbf{a}_2^*, \mathbf{b}_2^*, \mathbf{c}_2^*\}$ correspond to submultiples of the $K\alpha$ line for which the mass absorption coefficients of Cd and Cl atoms decay one order of magnitude. The weak sublattice was removed from the photographs using the same conditions of the IPDS generator.

[2] Supplementary data for this paper are available from the IUCr electronic archives (Reference: NA0098). Services for accessing these data are described at the back of the journal.

[3] 153 reflections [44 with $I > 3\sigma(I)$] in the range $-6 \leq h \leq 6$, $-6 \leq k \leq 6$. Approximate cell parameters were $a_2 = 34.64$ (3) and $b_2 = 34.46$ (2) Å.

4.2. Structure of phase I

Using the reflections corresponding to the strongest domain, the structure of phase I was solved and refined. Intensities were corrected carefully for absorption (analytical method based on the form of the crystal) and Lp. Data were averaged using different symmetries. The best internal R factor was achieved under the Laue symmetry $6/m$ (see Table 1). The coordinates of the unique independent Cd atom were easily found using direct methods. A difference-Fourier synthesis showed the positions of Cl and N atoms. Refinement of the atomic positions and anisotropic displacement parameters gave a residual factor $R = 0.15$. A new difference-Fourier map revealed electronic density residues around N atoms. However, there was not a clear indication about the correctness of any of the proposed models (2W, 3W or 6W) for the disordered TMA ions. In fact, all the models give the same final R factor (0.044) and nothing new appears with respect to the structure (2W splitting) published by Morosin (1972). The three models describe the same electronic density and although the population parameter and the positions of C atoms are different in each of them, their thermal ellipsoids adopt the appropriate shape and size to mimic three symmetry-related arcs of electronic charge around the N atoms (see Fig. 5). Atomic positions and displacement parameters corresponding to the 6W model are given in Table 3. As expected, analogous results were obtained for the refinements based on the intensities of the weaker domains. The way in which the organic tetrahedra are oriented is difficult to predict and it should be connected with the number of wells (in the sense of Frenkel models) used to decompose the electronic density around the N atoms. A closer description of the configuration of the C atoms in the average structure can be obtained by the maximum entropy method (MEM). MEM produces electron-density maps less biased by truncation effects and, therefore, sharper and less noisy than Fourier maps obtained in the same conditions. In the present case several MEM maps were calculated under the space groups $P6_3/m$ and $P6_3$ using the observed structure factors phased with a model including only Cd, Cl and N atoms. The maps (almost identical for both space groups) show the remaining atoms mainly located in a 2W configuration, *i.e.* the C atoms forming pairs of tetrahedra related by mirror planes and centred at points ($z = 0.25$ and $z = 0.75$) of average symmetry $3/m$ (see Fig. 6). There is no evidence of disorder on the mirror planes. Although the charge distribution out of the planes follows the configuration outlined by the anisotropic displacement parameters of C atoms, it is well located around the threefold axis.

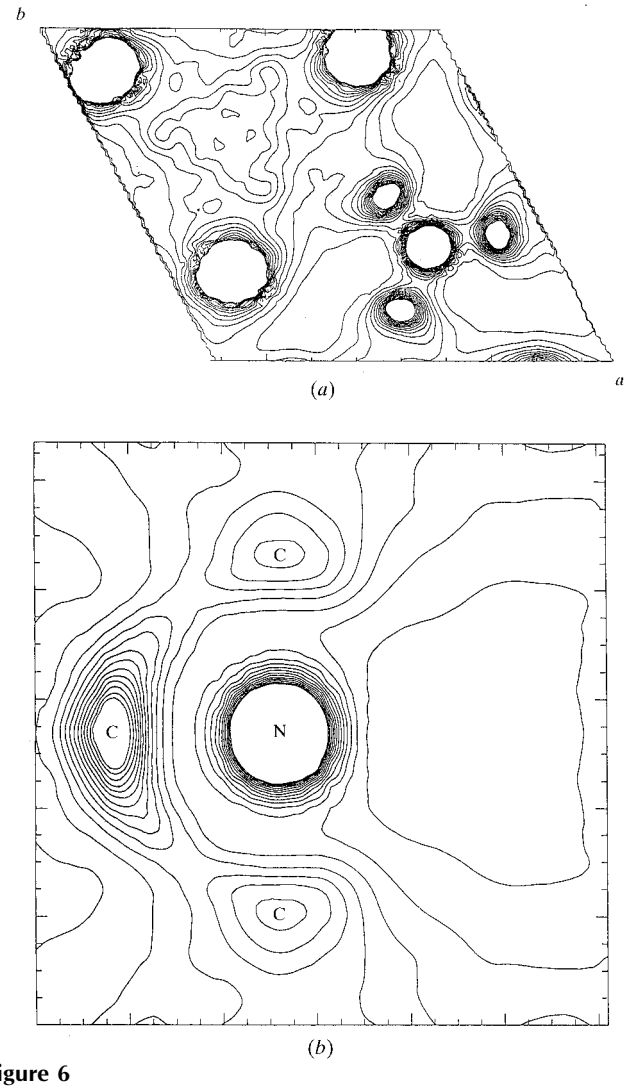

Figure 6
MEM sections of the unit cell showing the electronic density around the N atoms. (*a*) The $z = 0.25$ plane. (*b*) The section containing one of the C—N bonds and the threefold axis. Notice the absence of disorder on the mirror plane and the more diffuse distribution of electronic density in (*b*). Nevertheless, C atoms occupy roughly a 2W configuration (see text), *i.e.* they are predominantly located in the vicinity of the mirror plane and the threefold axis.

5. Study of the X-ray diffraction data from powdered samples

Powder diffraction diagrams were collected for the three phases and as shown in Fig. 7, the evidence of two phase transitions is clear. Attempts were made in order to solve the structures of phases II and III. For phase II, assuming the space group $P2_1/m$, the coordinates of the heavier atoms (see Table 4) were easily located by direct methods based on a set of integrated intensities extracted from a powder diffraction pattern ($5.00 < 2\theta < 105.02^\circ$). A difference-Fourier map showed two additional atoms (N and C in Table 4). However, the remaining C atoms could not be located. The refinement of the atomic coordinates using the Rietveld method (Rietveld, 1969) did not improve the result and the R factors were unacceptably high. Therefore, the incomplete structural model proposed for phase II has to be considered with caution. A similar trial of solving the structure of phase III failed.

6. Ferroelastic domains in phases II and III

The reversibility and sample independence of the splitting appearing in the diffraction patterns of phases II and III points out that its origin is structural. In both cases the whole

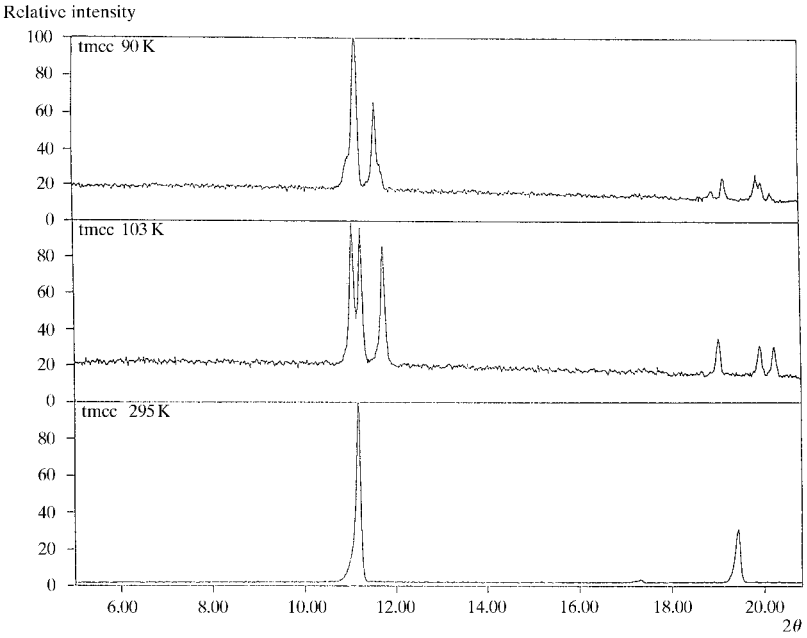

Figure 7
Powder diffraction patterns of the three phases I, II and III in the range $0 < 2\theta < 22^\circ$ showing the phase transitions.

diffraction pattern can be indexed with four identical domains (and eight additional domains obtained by successive applications of the threefold axis of phase I lost after the first phase transition) slightly misoriented. These four domains share the direction of $\mathbf{c}^*$ and are related by rotations of approximately 0 (domain *A*), 4 (*B*), 8 (*C*) and 12° (*D*) around this axis (see Fig. 8). Each of them would have the space group reported previously for each phase ($P2_1/m$, $Z = 2$ for phase II and $P2_1/b$, $Z = 12$ for phase III). In phase II the intensities of domains *B* and *C* are much stronger than those from domains *A* and *D*, whereas in phase III the intensity distribution is higher, but not more homogeneous, *i.e.* the relative volume of domains seems not to change after the transition between phases II and/or III. The usual way of calculating the number of orientational states and the coherent (plane) walls that separate one another (Sapriel, 1975) cannot predict the observed diffraction pattern. Assuming the correctness of the space groups assigned to the high- and low-temperature phases, 12 different orientational states could also be predicted if the intersection of the corresponding point groups were the trivial point group 1. However, it would imply in the diffraction pattern a three-dimensional distribution of spots, which is not observed in our case. The possibility of small angular misorientations of coherent domain walls around an axis common to all of them was also suggested by Sapriel (1975), although a quantitative method for calculating the rotation angle was given later by Shuvalov *et al.* (1985). The definition of coherent domain walls as planes whose points are equally distorted by the two orientational states that share them permits a very straightforward way of obtaining the rotation of the domain walls with respect to those predicted by Sapriel (1975). The rotation angles of the domains are connected with the absolute value φ of the eigenvalues[4] of $x(S_1) - x(S_2)$, $x(S_1)$ and $x(S_2)$ being the spontaneous strain tensors corresponding to the orientational states separated by a given coherent domain wall. As can be easily understood, this angle depends on the ferroelastic deformation and therefore on temperature. The domain walls calculated by Sapriel (1975) are preserved if the two domains rotate in opposite directions by $\varphi/2$. However, it should be noted that in general, owing to these rigid rotations of the domains the number of spots present in a single-crystal diffraction diagram will be higher than expected. Notice also that this formalism does not predict the actual distribution of domains and coherent domain walls. That can only be deduced from a diffraction experiment.

For our particular case, the structural phase transition from phase I to phase II belongs to the ferroelastic species $6/mF2/m$ (Aizu, 1970). Setting the z axis along the sixfold axis of the prototypic phase and the y axis perpendicular to z and parallel to the (common for both phases) **b** axis, the spontaneous strain tensors for the three orientational states, S_1, S_2 and S_3, have the following form

$$x(S_1) = \begin{pmatrix} e_{11} & e_{12} & 0 \\ e_{12} & e_{22} & 0 \\ 0 & 0 & 0 \end{pmatrix}$$

$$x(S_2) = \begin{pmatrix} \frac{e_{11}+3e_{22}}{4} - \frac{3^{1/2}}{2}e_{12} & -\frac{3^{1/2}}{4}(e_{22}-e_{11}) - \frac{e_{12}}{2} & 0 \\ -\frac{3^{1/2}}{4}(e_{22}-e_{11}) - \frac{e_{12}}{2} & \frac{3e_{11}+e_{22}}{4} + \frac{3^{1/2}}{2}e_{12} & 0 \\ 0 & 0 & 0 \end{pmatrix}$$

$$x(S_3) = \begin{pmatrix} \frac{e_{11}+3e_{22}}{4} + \frac{3^{1/2}}{2}e_{12} & \frac{3^{1/2}}{4}(e_{22}-e_{11}) - \frac{e_{12}}{2} & 0 \\ \frac{3^{1/2}}{4}(e_{22}-e_{11}) - \frac{e_{12}}{2} & \frac{3e_{11}+e_{22}}{4} - \frac{3^{1/2}}{2}e_{12} & 0 \\ 0 & 0 & 0 \end{pmatrix}.$$

To avoid the effect of thermal expansion the lattice parameters of the high-temperature phase normally have to be extrapolated to the temperature where the cell parameters of the ferroelastic structure are known. A common way of doing such extrapolation involves defining an 'average' structure characterized by the arithmetic mean of all possible strain tensors in the low-symmetry phase. In our case, the average structure is defined by

$$x_{av} = \begin{pmatrix} (e_{11}+e_{22})/2 & 0 & 0 \\ 0 & (e_{11}+e_{22})/2 & 0 \\ 0 & 0 & 0 \end{pmatrix},$$

[4] It can be shown (Shuvalov *et al.*, 1985) that the eigenvalues of $x(S_1) - x(S_2)$ are $0 \pm \varphi$.

where (Salje, 1990)

$$e_{11} = (a \sin\gamma / a_o \sin 120^\circ) - 1$$

$$e_{22} = (b/a_o) - 1$$

$$e_{12} = \left(\tfrac{1}{2}\right)\left(\frac{a\cos\gamma}{a_o \sin 120^\circ} - \frac{b\cos 120^\circ}{a_o \sin 120^\circ}\right).$$

a, b, γ and a_o are the relevant cell parameters of the low- and (the extrapolated) high-symmetry phases, respectively. The condition that these tensor components vanish in the average structure (*i.e.* the extrapolated hexagonal structure at low temperature) becomes:

$$(e_{11} + e_{22})/2 = \left(\tfrac{1}{2}\right)\left(\frac{a\sin\gamma}{a_o \sin 120^\circ} + \frac{b}{a_o} - 2\right) = 0$$

and therefore

$$a_o = \frac{a\sin\gamma + b\sin 120^\circ}{2\sin 120^\circ}.$$

Taking into account the value of a_o, the form of the three spontaneous strain tensors are

$$x(S_1) = \begin{pmatrix} -a & b & 0 \\ b & a & 0 \\ 0 & 0 & 0 \end{pmatrix}$$

$$x(S_2) = \begin{pmatrix} -(-a/2 + b(3)^{1/2}/2) & -b/2 - a(3)^{1/2}/2 & 0 \\ -b/2 - a(3)^{1/2}/2 & -a/2 + b(3)^{1/2}/2 & 0 \\ 0 & 0 & 0 \end{pmatrix}$$

$$x(S_3) = \begin{pmatrix} -(-a/2 - b(3)^{1/2}/2) & -b/2 + a(3)^{1/2}/2 & 0 \\ -b/2 + a(3)^{1/2}/2 & -a/2 - b(3)^{1/2}/2 & 0 \\ 0 & 0 & 0 \end{pmatrix}$$

with $a = (e_{22} - e_{11})/2$ and $b = e_{12}$. Then the difference of spontaneous strain tensors $x(S_1) - x(S_2)$ [the same results are obtained if $x(S_1) - x(S_3)$ or $x(S_2) - x(S_3)$ are used] can be written as follows

$$\Delta x = x(S_1) - x(S_2) = \begin{pmatrix} -(-3a/2 - b(3)^{1/2}/2) & -3b/2 - a(3)^{1/2}/2 & 0 \\ 3b/2 - a(3)^{1/2}/2 & 3a/2 + b(3)^{1/2}/2 & 0 \\ 0 & 0 & 0 \end{pmatrix}.$$

In this case the values of the rotation angle of the orientational states (Shuvalov *et al.*, 1985) will be equal to or a multiple of $\varphi = [3(a^2 + b^2)]^{1/2}$. Therefore, for phase II at 103 K, the theoretical value for φ is 3.5 (1)°. The experimental value of this rotation angle is 3.6 (2)°. On the other hand, recent ^{35}Cl NMR measurements in phase II of TMCC reveal an unexpected splitting of the NMR lines corresponding to small rotations around the pseudo-hexagonal axis of ∼4° (Mulla-Osman *et al.*, 1998). This splitting cannot be explained by another assignation of the space groups involved. However, their measurements can be explained properly by our model of domain structure assuming that only the two most prominent domains (*B* and *C*) are being detected. The ferroelastic domains observed in phase III are inherited from those of phase II. The theoretical value of φ for phase III can be calculated assuming that its variation is only due to the temperature change of lattice parameters. Under this assumption the sequence of structural phase transitions for TMCC

$$\begin{array}{ccc} P6_3/m & \Longrightarrow P2_1/m & \Longrightarrow P2_1/b \\ a_{\rm I}, b_{\rm I}, c_{\rm I} & a_{\rm II}, b_{\rm II}, c_{\rm II} & a_{\rm III}, b_{\rm III}, c_{\rm III} \\ Z = 2 & Z = 2 & Z = 12 \end{array}$$

is completely equivalent to the following sequence

$$\begin{array}{ccc} P6_3/m & \Longrightarrow P2_1/m & \Longrightarrow P2_1/b \\ a_{\rm I}, b_{\rm I}, c_{\rm I} & a_{\rm III}, b_{\rm III}/2, c_{\rm II} & a_{\rm III}, b_{\rm III}, c_{\rm III} \\ Z = 2 & Z = 2 & Z = 12 \end{array}$$

Hence, the value of φ for phase III can be calculated by appropriately transforming the lattice parameters of phase III to the cell of phase II. In this case the theoretical and measured values of φ are 2.6 (1) and 2.5 (2)°, respectively. TMCC is not the only compound of this family that presents anomalous diffraction patterns in the low-temperature phases. The related compounds $(CH_3)_4NMnBr_3$ (TMMB; Visser & McIntyre, 1989) and $(CH_3)_4NNiBr_3$ (TMNB; Knop & Steiner, 1984) also exhibit diffraction diagrams that can only be indexed with at least two (symmetry-independent) misoriented domains. Their origin has been always considered as 'normal' in a ferroelastic phase transition. TMMB undergoes a ferroelastic phase transition at 144 K from $P6_3/m$ [a = 9.2040 (5), c = 6.7768 (7) Å] to $P2_1/m$ or $P2_1$ [a = 8.995, b = 6.777, c = 8.847 Å, β = 114.48°]. Single crystal neutron diffraction diagrams below 144 K (Visser & McIntyre, 1989) show a splitting of the reflections that can only be indexed with six monoclinic domains. This domain structure is considered by the authors as being due to the symmetry breaking at the phase transition point. Obviously this interpretation is incorrect since the number of ferroelastic domains given the involved point groups is 3. As this structural phase transition belongs to the same ferroelastic species as that of TMCC, the same procedure can be applied to this compound. In this case the value of φ is equal to 5.5 (1)°, which agrees nicely with the angle (about 5°) observed in Fig. 1 of Visser & McIntyre (1989). This angle has also been measured by antiferromagnetic resonance below the structural phase transition (Teraoka *et al.*, 1995). When the direction of the magnetic field is rotated in the hexagonal basal plane, three pairs of resonance signals are detected. The existence of the three pairs of resonance lines is attributed to the monoclinic twinning of the crystals. Each pair of lines are separated by ∼5.5°.

Something similar happens in the neutron scattering study of TMNB (Knop & Steiner, 1984), where at low temperatures the nuclear reflections were found to split. The phase transition is characterized by an increase of 3.5° in γ without changes in the length of the a and b axes. The splitting was simply explained as originating from a hexagonal–monoclinic ferroelastic phase transition. Again the explanation is not

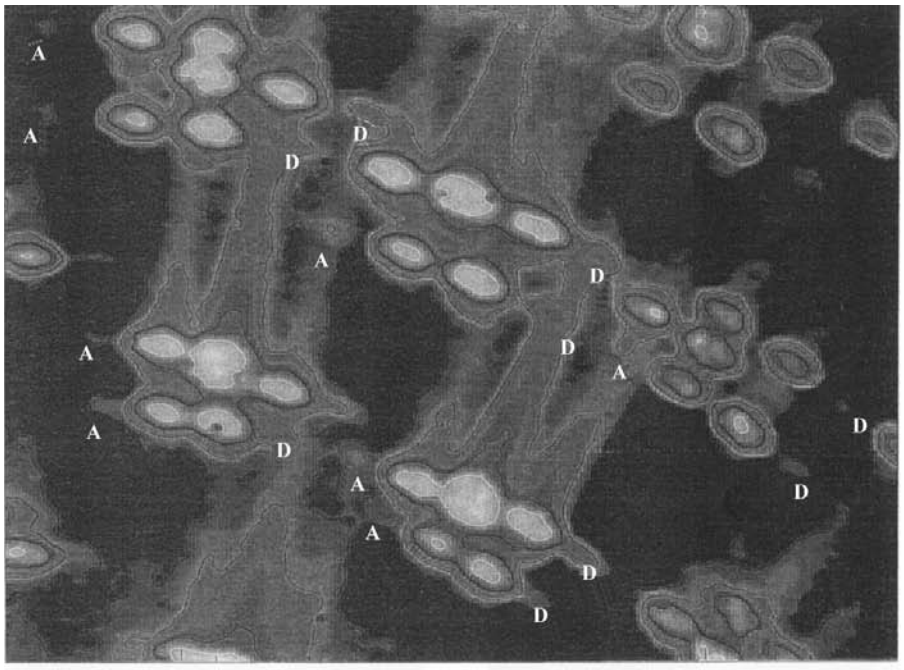

(*a*)

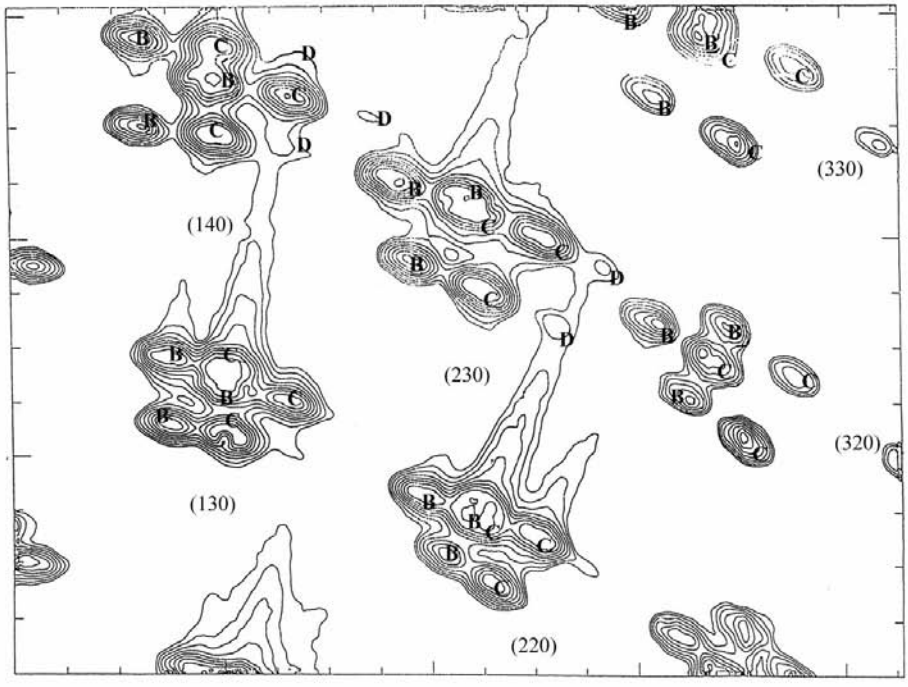

(*b*)

Figure 8
Scan of a small region of a (*hk*0) precession photograph at 103 K. (*a*) Gray map; (*b*) contour map based on (*a*). Miller indices appearing in (*b*) correspond to the (*hk*0) reflections on which each bunch of reflections converge after the phase transition to phase I. All the reflections can be indexed with four domains labelled *A*, *B*, *C* and *D* (see text). Reflections belonging to the weaker domains (*A* and *D*) can be clearly seen in (*a*).

entirely correct. It can be shown that the theoretical value of φ again coincides properly with the angle shown in Fig. 1 of Knop & Steiner (1984). This misalignment of coherent domain walls is not a particular feature of the TMCC family. Other examples are the hexagonal–orthorhombic transition in urea inclusion compounds (Boysen, 1995) and the cubic tetragonal transition in leucite (Korekawa, 1969). In these materials more domains than predicted from the group–subgroup relationship between the two phases again appear. In both cases the appearance of additional domains are considered as a mechanism for reducing strains at the domain interfaces. Boysen (1995) gives a value for φ, calculated from geometrical considerations, that coincides (for small angles) with the expression given by Shuvalov *et al.* (1985).

7. Conclusions

The diffraction diagrams of phases I, II and III of TMCC exhibit peculiar features, some of them never reported and correctly explained for other members of the $(CH_3)_4NMX_3$ family. First, the number of domains needed to explain the diffraction patterns (and the NMR results) of the low-temperature phases is too high to be due to symmetry breaking at the phase transition temperature. The orientation of the extra domains induced by strain relaxation at the domain walls has been calculated from the ferroelastic distortion and explains the experimental results at low temperatures. On the other hand, the kind of disorder of TMA at room temperature is still a question to be solved. MEM points towards a 2W configuration for the disordered TMA groups. If this disorder is static the refined configurations of TMA at room temperature would mimic a spatially averaged 'up–down' sequence(s)[5] of the organic groups. The very complicated single-crystal diffraction diagrams of phases II and III prevent an accurate data collection and therefore any attempt at structure solution. This difficulty can be partially overcome by means of powder diffraction techniques. Although the structure of phase II has not been properly refined, the change in symmetry seems to be related (at least

[5] 'Up' and 'down' would refer to the orientation, with respect to *c*, of the vector joining the central N atom and the apices of the tetrahedra situated on the threefold axis

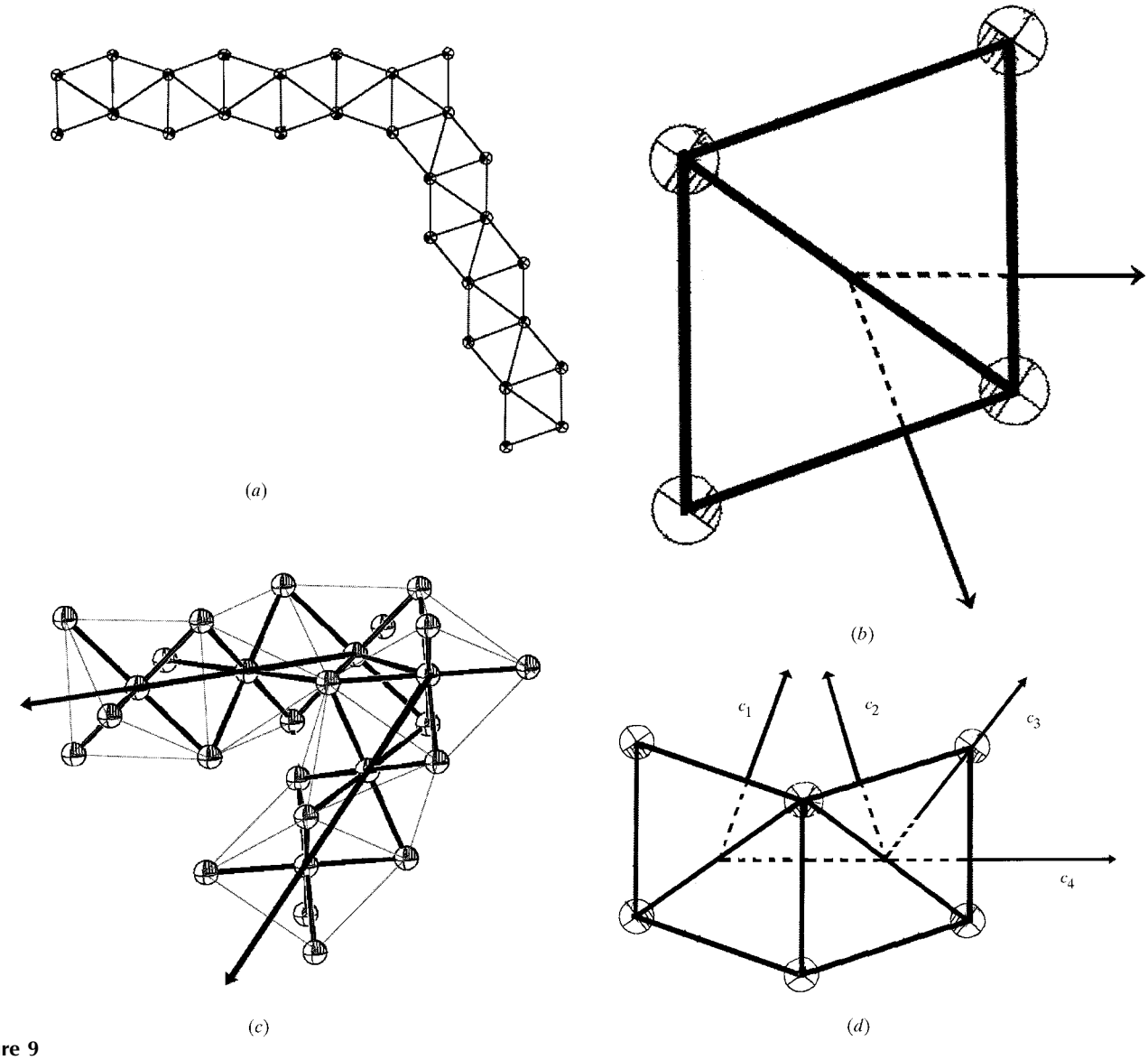

Figure 9
(*a*) Projection along [110] of a chain of $CdCl_6$ octahedra showing a possible sharing-faces stacking defect that provokes the tilting of the **c** axis. (*b*) In this case the angle of tilt is reduced to the angle between any two adjacent faces of one octahedron ∼72°. (*c*) Projection of a chain of $CdCl_6$ octahedra showing a possible stacking defect involving a second torsion. The **c** axes are indicated by arrows. (*d*) Now the possible angles of tilt are $\widehat{\mathbf{c}_1,\mathbf{c}_4} \simeq 72^\circ$ [as in (*b*)], $\widehat{\mathbf{c}_1,\mathbf{c}_3} \simeq 58^\circ$ and $\widehat{\mathbf{c}_1,\mathbf{c}_2} \simeq 33^\circ$.

in part) to a small change in Cl positions, which are no longer related by the threefold axis. An analysis of the positional changes of Cl atoms by NMR is in progress. Another marginal point to be ellucidated is the origin of the domains detected at room temperature. Since the **c** axis is parallel to the chains of $CdCl_6$ octahedra, an intuitive mechanism for the appearance of the observed domain structure would be the presence of stacking defects that would provoke the tilting of such an axis. Assuming that two adjacent octahedra always share one face, the different orientations of **c** are determined, in a first approximation, by the lines joining the centre of one octahedron with the centres of its faces. The only possible angle is ∼72° (see Figs. 9*a* and *b*). If a second torsion of the chain is allowed, the possible angles are ∼33 or 58° (Figs. 9*c* and *d*). As can be seen in Table 2, some of these angles agree with the measured ones, however, this simple model cannot reproduce all the measured angles. Anyway they seem not to influence the distribution of the ferroelastic domains at lower temperatures.

Authors gratefully acknowledge Professor D. Michel (University of Leipzig) for supplying the samples used by his group for NMR measurements. AP and IP are indebted to the Basque Government for financial support. This work has been supported by the Basque Government project no PI97/71.

References

Aguirre-Zamalloa, G., Madariaga, G., Couzi, M. & Breczewski, T. (1993). *Acta Cryst.* B**49**, 691–698.
Aizu, K. (1970). *J. Phys. Soc. Jpn*, **28**, 706–716.
Boysen, H. (1995). *Phase Transit.* **55**, 1–16.

Braud, M. N., Couzi, M., Chanh, N. B., Courseille, C., Gallois, B., Hauw, C. & Meresse, A. (1990). *J. Phys. Condens. Matter*, **2**, 8209–8228.
Cosier, J. & Glazer, A. M. (1986). *J. Appl. Cryst.* **19**, 105–107.
Couzi, M. & Mlik, Y. (1986). *J. Raman Spectrosc.* **17**, 117–124.
Davenport, G., Hall, S. & Dreissig, W. (1992). *ORTEP. Xtal3.2 Reference Manual*, edited by S. R. Hall, H. D. Flack and J. M. Stewart. Universities of Western Australia, Australia, Geneva, Switzerland, and Maryland, USA.
Dreissing, W., Doherty, R., Stewart, J. & Hall, S. (1992). *Xtal*3.2 *Reference Manual*, edited by S. R. Hall, H. D. Flack & J. M. Stewart. Universities of Western Australia, Australia, and Maryland, USA.
Enraf–Nonius (1996). *CAD*-4*VPC*. Version 2.0. Enraf–Nonius, Delft, The Netherlands.
Gesi, K. (1992). *Ferroelectrics*, **137**, 209–223.
Hall, S. R., Flack, H. D. & Stewart, J. M. (1992). *Xtal3.2 Reference Manual.* Universities of Western Australia, Australia, Geneva, Switzerland, and Maryland, USA.
Jewess, M. (1982). *Acta Cryst.* B**38**, 1418–1422.
Knop, W. & Steiner, M. (1984). *Solid State Commun.* **51**, 521–524.
Korekawa, M. (1969). *Z. Kristallogr.* **129**, 343–350.
Mlik, Y. & Couzi, M. (1982). *J. Phys. C*, **15**, 6891–6906.
Morosin, B. (1972). *Acta Cryst.* B**28**, 2303–2305.
Morosin, B. & Graeber, E. J. (1967). *Acta Cryst.* **23**, 766–770.
Mulla-Osman, S., Michel, D., Czapla, Z. & Hoffmann, W. D. (1998). *J. Phys. Condens. Matter*, **10**, 2465–2476.
Olthof-Hazekamp, R. (1992). *Xtal*3.2 *Reference Manual*, edited by S. R. Hall, H. D. Flack & J. M. Stewart. Universities of Western Australia, Australia, and Maryland, USA.
Peercy, P. S., Morosin, B. & Samara, G. A. (1973). *Phys. Rev. B*, **8**, 3378–3388.
Rietveld, H. M. (1969). *J. Appl. Cryst.* **2**, 65–71.
Rodriguez, V., Aguirre-Zamalloa, G., Couzi, M. & Roisnel, T. (1996). *J. Phys. Condens. Matter*, **8**, 969–981.
Rodriguez, V., Guillaume, F. & Couzi, M. (1996). *J. Phys. Chem.* **100**, 14109–14117.
Salje, E. K. H. (1990). *Phase Transitions in Ferroelastic and Co-elastic Crystals*, pp. 25–26. Cambridge University Press.
Sapriel, J. (1975). *Phys. Rev. B*, **12**, 5128–5139.
Shuvalov, L. A., Dudnik, E. F. & Wagin, S. V. (1985). *Ferroelectrics*, **65**, 143–152.
Teraoka, S., Kambe, T., Koido, N., Hirai, S. & Nagata, K. (1995). *J. Magn. Magn. Mater.* **140–144**, 1659–1660.
Visser, D. & McIntyre, G. J. (1989). *Physica B*, **156/157**, 259–262.